

BROADBAND POLARIZATION CONVERSION BASED ON SMALL-SIZE METAMATERIAL IN THE GHz BAND

Duong Thi Ha^{1,3}, Tran Quoc Ve³, Dinh Ngoc Dung^{1,4}, Bui Son Tung^{1,2},
Nguyen Thi Hien⁵, Vu Thi Hong Hanh³, Bui Xuan Khuyen^{1,2, **}, Vu Dinh Lam^{1,2, *}

¹Graduate University of Science and Technology (GUST), VAST, Cau Giay,
18 Hoang Quoc Viet, Ha Noi, Viet Nam

²Institute of Materials Science, VAST, 18 Hoang Quoc Viet, Cau Giay, Ha Noi, Viet Nam

³Department of Physics, Thai Nguyen University of Education, Thai Nguyen, Viet Nam

⁴Faculty of Materials Science and Engineering, Phenikaa University, Yen Nghia, Ha Dong,
Ha Noi 12116, Viet Nam.

⁵Faculty of Physics and Technology, TNU- University of Sciences, Tan Thinh Ward,
Thai Nguyen City, Viet Nam

*Email: lamvd@gust-edu.vast.ac.vn. **Email: khuyenbx@ims.vast.ac.vn

Received: 15 January 2021; Accepted for publication: 9 September 2021

Abstract. We proposed a small GHz metamaterial perfect absorber, which can operate in two different functional modes depending on the orientation of unit-cell structure. Firstly, when the unit-cell structure is oriented symmetrically to the external electric-field direction, an absorption mode is achieved with a near-perfect absorption peak (absorption of 99 % at 13.9 GHz). Secondly, by rotating the resonator structure on top layer, metamaterial is asymmetric to the external field, leading to the excitation of cross-coupling effect. Consequently, a polarization-conversion mode is obtained with a high cross-polarization reflection in a broadband region (where the cross-polarization coefficient reaches up to 75 % in the frequency-range of 12.5 - 16.5 GHz). The polarization conversion was verified by experiment and the mechanism was clarified by the simulation of induced electric and magnetic fields. Our work could contribute to metamaterial-based multifunctional devices such as filter and polarization modulators.

Keywords: metamaterial, polarization conversion, broadband.

Classification number: 2.1.2, 2.2.2, 2.10.1.

1. INTRODUCTION

In the last few decades, Metamaterials (MMs) have attracted a great deal of attention. MM is an artificial material, consisting of pseudo-atoms (resonant structures) that are 7 to 10 times smaller than the operating wavelength. The biggest advantage of MMs is that they can be

designed to achieve desired electromagnetic (EM) properties, including: the negative refractive index [1, 2], the reverse Cherenkov effect [3] and the reverse Doppler effect [4] that do not exist in nature. The development history of MM dates back to 1968 when Veselago first predicted the extraordinary EM properties of a medium that simultaneously possessed the negative effective permeability and permittivity [5]. More than two decades later, MM with a negative index of refraction was verified experimentally by Smith *et al.* [6]. In 2008, Landy *et al.* proposed a metamaterial perfect absorber (MPA) [7] which had outstanding advantages in thickness (30 times smaller than absorption wavelength) compared to the other traditional absorbent materials. Since then, research on MMs has grown dramatically with a wide range of potential applications such as invisibility cloaks [8], super lenses [9, 10], filters [11] and sensors [12 - 14].

Additionally, the ability of MMs to convert the polarization state of incident light has also received a great attention. Polarization is an important feature of the EM wave which refers to the orientation of electric field component in space. Manipulating the polarization state of EM wave is essential due to its various applications in the signal transmission and the sensitive measurement. The polarization state can be controlled using conventional polarization converters made of anisotropic materials, such as natural birefringent crystals, mirror asymmetric materials and magnetized plasmas. However, these converters have bulky volumes and narrowband frequency response, making them unsuitable for realizing ultrathin device sensors and nanophotonic devices [15]. Recently, to overcome these limitations, a new type of device based on MMs has been proposed to achieve the polarization conversion with single-/multi- and ultra-broadband and miniaturized structures [15 - 20].

Recently, single-/multi- and broad-band operations of EM-polarization converters and MPAs are being intensively suggested for next generations of polarization switching, solar energy harvesting, integrated polarization conversion, radar cross section (RCS) reduction and photo-detection [21 - 24]. However, most conventional MM-based devices are still designed by complex structures that make it a difficult task to commercialize. For this motivation, in this paper, we propose a simple planar polarization conversion structure consisting of asymmetric resonators. Due to the cross-coupling between induced field and incident wave, near complete and broadband polarization conversion can be achieved. The absorption properties of this structure were also numerically simulated and experimentally investigated to provide a deeper insight into the mechanism of our structure.

2. SIMULATION, FABRICATION AND MEASUREMENTS

The schematic diagram of the proposed model with its sub-wavelength unit cell was optimized and shown in Fig. 1a. In general, in the GHz band, the MM unit cell consists of three layers: a patterned-copper layer (for selecting the operational frequency), a dielectric substrate (for providing effective absorption/reflection volume) and a continuous copper layer (for blocking the EM transmission). In simulation, therefore, the dielectric substrate was made by FR-4 with a thickness of 0.38 mm, a relative dielectric constant of 4.3 and a loss tangent of 0.025. Both the patterned layer and the continuous layer have an electric conductivity of 5.96×10^7 S/m and a thickness of 0.035 mm. The top patterned layer of the unit cell contains a split-ring resonator (SRR) combined with a cut-wire structure. The lattice constant of the unit cell in both x and y directions is $a = 4$ mm and the geometrical parameters of the unit cell are given by d_0 , d_i , d , w and l , as shown in Fig. 1a. Our simulation was carried out by using the commercial CST-Microwave Studio software. The frequency domain solver was used with the frequency range from 12 to 18 GHz while unit cell boundary is applied for both x and y

direction. In our simulation, the electric-field vector and the magnetic-field vector of incident EM wave are oriented along to the y -axis and x -axis, respectively (for the TE mode).

For our experiment, the photolithography technique was used to fabricate a sample with 525 unit cells. The fabrication process included four main steps: firstly, the photoresistant agent was coated on a printed-circuit-board (PCB) and a photomask with the pre-designed structure was placed on the photoresistant layer. The system was then exposed to light for the appropriate time. In the second step, the photoresistant substances, which were not illuminated in the first step, were removed by the developed solvent. In the etching step, the liquid chemical agent removed the upper metallic layer in the area not protected by the photoresistant to obtain the desired structure. Finally, the remaining photoresistant was removed.

The transmission and reflection coefficients of the fabricated sample were measured by a vector network analyzer (Rohde & Schwarz ZNB20) (Fig. 1c). The measuring system consists of two identical linearly polarized standard-gain horn antennas as the transmitter and the receiver, as shown in Fig. 1c. The absorptivity $A(\omega)$ of a material is defined as $A(\omega) = 1 - R(\omega) - T(\omega)$, where $T(\omega) = |S_{21}|^2$ and $R(\omega) = |S_{11}|^2$ are the transmission and reflectance coefficients, respectively, while $|S_{11}|^2$ and $|S_{21}|^2$ are correspondingly the scattering parameters of the reflection and the transmission.

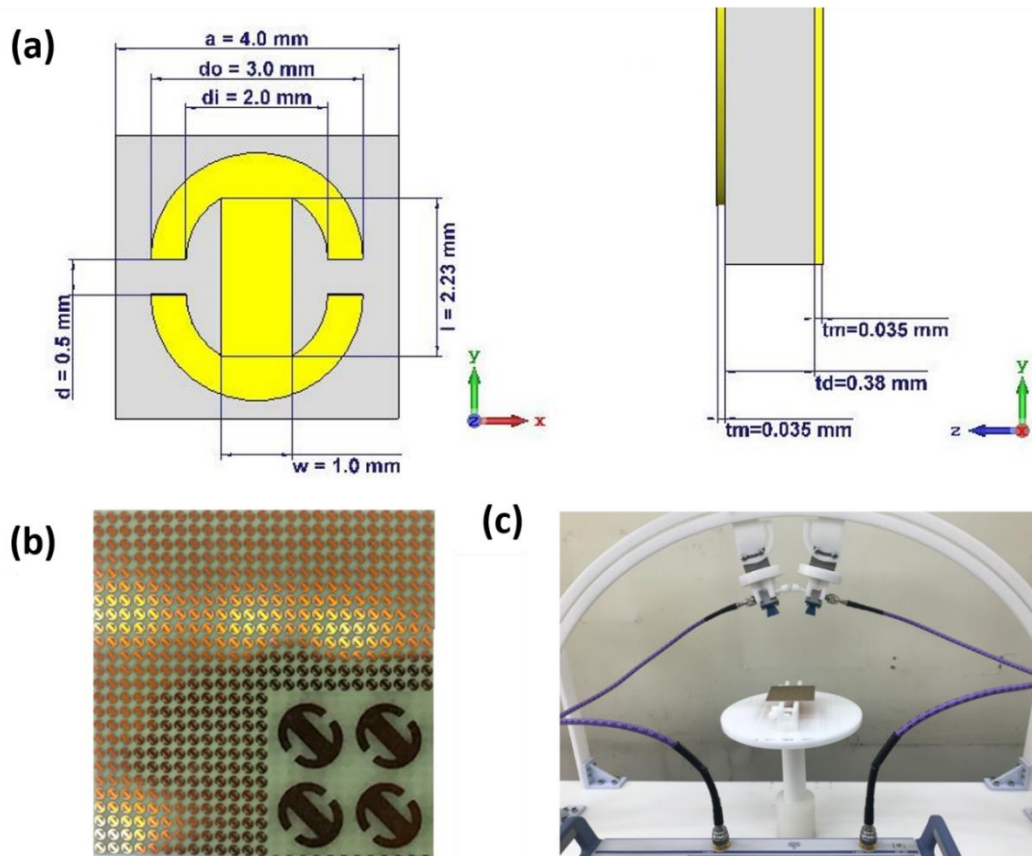


Figure 1. (a) Schematic diagram of the proposed unit cell. (b) Full-size fabricated sample and (c) corresponding measurement configuration, by using the Vector Network Analyzer ZNB20.

3. RESULTS AND DISCUSSION

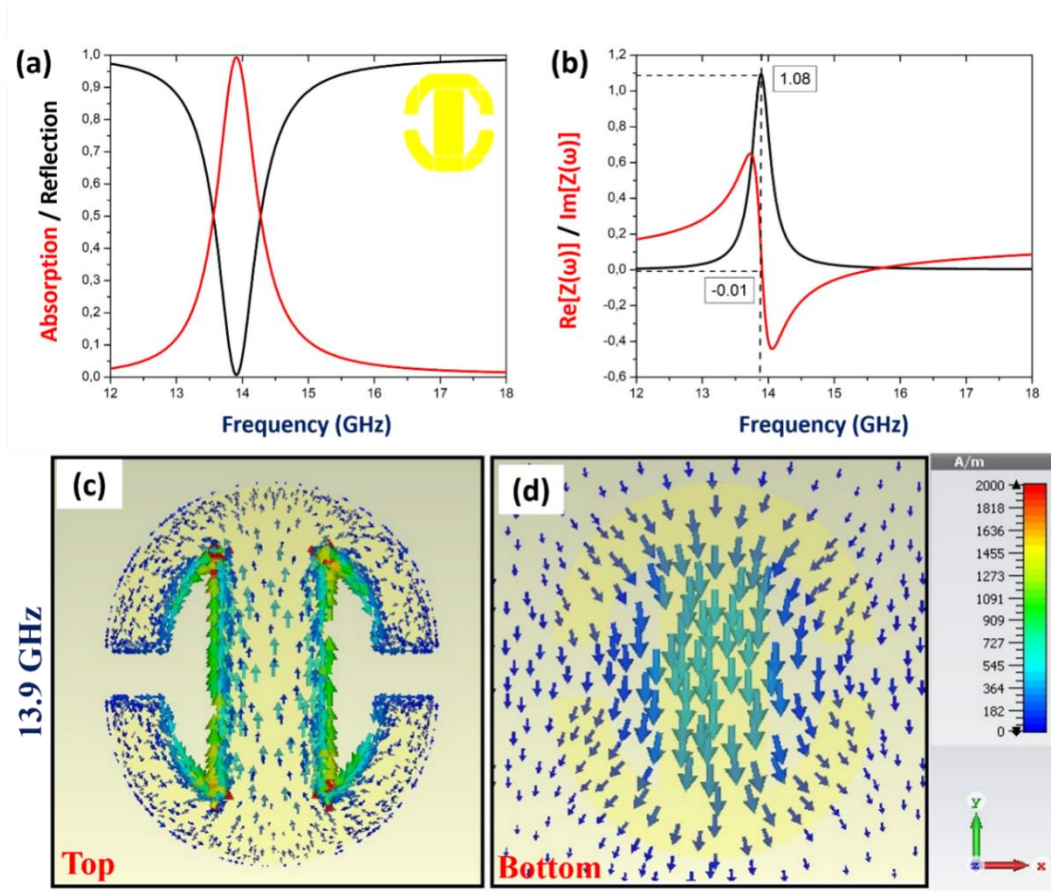


Figure 2. (a) Simulation results of co-polarized reflection and co-polarized absorption coefficients of the MPA structure, symmetrically oriented in the polarization axis of the electric field. (b) Normalized impedance and distributions of surface current on (c) the top and (d) bottom layers for normal incidence at 13.9 GHz.

Firstly, we considered the MPA structure, symmetrically oriented in the polarization axis of the electric field. Figure 2 presents simulation results of co-polarized reflection and absorption of the normal incident TE wave. The co-polarized reflection and co-polarized absorption can be calculated by the following expressions:

$$\begin{aligned}
 A_{co-polarized} &= 1 - R_{yy} - T_{yy} \\
 &= 1 - |S_{1y,1y}|^2 - |S_{2y,1y}|^2 \\
 &= 1 - |S_{1y,1y}|^2,
 \end{aligned} \tag{1}$$

$$R_{co-polarized} = R_{yy} = |S_{1y,1y}|^2, \tag{2}$$

where $S_{1y,1y}$ and $S_{2y,1y}$ are the reflection and transmission coefficients, respectively, when both the transmitting and receiving antennas were in the TE mode. The bottom layer was covered with a copper continuous layer, therefore, the transmittance component can be neglected

($T_{yy} = 0$). As shown in Fig. 2a, the co-polarized reflection coefficient is minimized to near 0 at 13.9 GHz. According to Eq. (1), the absorption spectrum exhibits a single resonant peak at this resonant frequency with an absorbance of 99 %. The mechanism of the MM absorber was also clarified by calculating the impedance of this structure (Fig. 2b). It is shown that the real part of the relative impedance at the resonant frequency is 1.08, which implies that the impedance matching condition is satisfied. Therefore, at the resonant frequency, the EM waves are not reflected at the top layer of this structure and propagate entirely into the material.

To have a better physical view of the mechanics of absorption, the distribution of induced surface currents on the two metallic layers at the resonant frequency is also studied. As shown in Figs. 2c and 2d, the current distribution mainly accumulates on the cut wire structure. The surface currents of the top and bottom layers have opposite directions, which implies that this resonance peak is magnetic [25]. This magnetic resonance together with the aforementioned impedance matching condition proves its ability to act as a perfect absorber in this case.

To evaluate the effect of changing the orientation of the proposed structure on its respond to EM waves, the structure was rotated 45° , as shown in Fig. 3a. Figure 3b shows the co-polarized absorption of the proposed MPA structure when the thickness of the FR-4 layer varies from 0.38 mm to 1.2 mm, while other parameters are kept constant. It is observed that, at $t_d = 1.2$ mm, a broadband absorption spectrum can be achieved due to the combination of two resonant peaks at 12.9 and 15.9 GHz. Therefore, to meet the optimization purpose, the thickness of the dielectric substrate was optimized to be 1.2 mm.

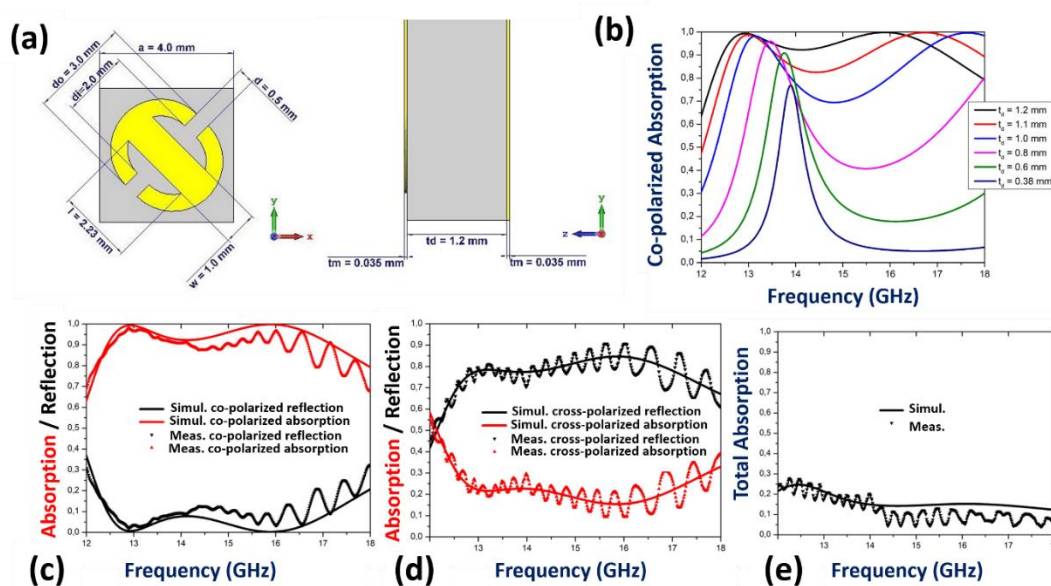


Figure 3. (a) Orientation of asymmetric structure. (b) Dependence of the co-polarized absorption coefficient on the dielectric layer thickness. Simulation and measurement results of (c) co-polarized reflection and absorption coefficients, (d) cross-polarized reflection and absorption coefficients and (e) total absorption.

Figure 3 presents the results of simulation and measurement total absorption; co- and cross-polarized absorption, co- and cross-polarized reflection coefficients of the MPA structure. These co-polarized absorption and co-polarized reflection coefficients are calculated by using Eqs. (1)

and (2), while cross-polarized absorption and cross-polarized reflection coefficients are determined by the following expressions:

$$\begin{aligned}
 A_{cross-polarized} &= 1 - R_{xy} - T_{xy} \\
 &= 1 - |S_{1x,1y}|^2 - |S_{2x,1y}|^2 \\
 &= 1 - |S_{1x,1y}|^2
 \end{aligned}$$

$$R_{cross-polarized} = R_{yx} = |S_{1x,1y}|^2 \quad (3)$$

$$\begin{aligned}
 A_{total} &= 1 - R_{xy} - R_{yy} - T_{xy} - T_{yy} \\
 &= 1 - |S_{1x,1y}|^2 - |S_{1y,1y}|^2
 \end{aligned}
 \quad (4)$$

where $S_{1x,1y}$ and $S_{2x,1y}$ are the reflection and transmission coefficients, respectively. It should be noted that, in our investigation, the transmitting antenna emits the TE-EM waves and the receiving antenna detects the TM-EM waves.

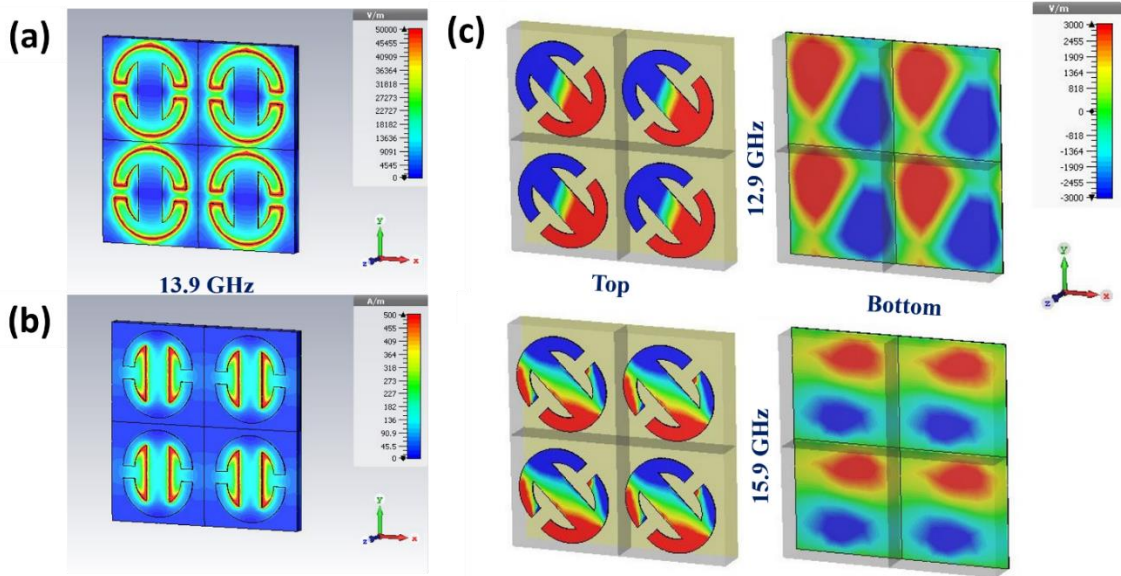


Figure 4. Distribution of: electric field (a), magnetic field (b) on symmetric MPA structure and (c) the distribution of electric field on asymmetric MPA structure.

As shown in Fig. 3c, both simulation and experimental results are in good agreement, where there is a broadband co-polarized absorption spectrum, from 12.5 to 16.5 GHz with an average absorption of 98 % (from 95 - 100 %). This broadband absorption spectrum is caused by the combination of two resonant peaks at 12.9 and at 15.9 GHz. However, the energy of the EM waves absorbed by the proposed MPA structure is not simply converted to heat as in recent MPAs [7, 26 - 28], because as shown in Fig. 3d, a part of the EM wave energy (above 75 %) is reflected in cross-polarization. It means that the proposed structure is capable of converting y-polarized EM waves into x-polarized ones. The total absorption when taking into account the contributions of both co- and cross-polarized reflections is only approximately 0.2, as shown in Fig. 3e. In particular, the actual unit cell thickness of the proposed structure is scaled to: $t_d/\lambda = 0.05$ (at 12.9 GHz). These values confirm that our structure is thinner than other common MMs [29, 30]. The slight deviation between the simulated results and the measured

ones can be attributed to the relatively large apertures of the two horn antennas in the measurement at 50° incident angle of the incoming EM wave, as shown in Fig. 1c.

To clarify the polarization switching mechanism in our designed structure, the distributions of electric and magnetic fields are studied and presented in Fig. 4. As shown in Fig. 4a, the electric field is mainly distributed in the outer edge of the SRR, while the magnetic field is enhanced around the wire-cut area. In addition, the induced electric and magnetic fields are symmetrically distributed across both the x and y axes in the MPA symmetric structure. In the case of asymmetric structure, the simulated induced electric field is shown in Fig. 4c. At the resonant frequency of 12.9 GHz, the magnitude of electric field is only symmetrical across the u axis, inclined 45° to the y axis, but opposite in sign, while at the frequency of 15.9 GHz, the distribution of electric field is symmetrical across the v axis, inclined -45° to the v axis. In both resonant frequencies, the signs of the electric fields of the top and bottom metal layers remain opposite, indicating that both resonances at 12.9 and 15.9 GHz are magnetic. Furthermore, it should be noted that, the optimization of the substrate thickness has the role pulling the two resonant peaks together to create a broadband region. Therefore, the interaction between these two resonances (which causes the direction of the field at 15.9 GHz) is not completely perpendicular to the structural axis.

The cross-coupling effect between the induced field and the incident wave field is used to explain the polarization conversion mechanism [31, 32]. In the symmetric structure, the distribution of electric and magnetic fields is symmetrical across the electric vector and magnetic vector direction of the incident EM wave. Therefore, the cross-coupling does not exist in this case. Consequently, the symmetric structure does not exhibit polarization conversion effect. In contrast, the induced fields in the asymmetrical structure are not symmetric across the external fields, so the cross-coupling can be created between them. At the resonant frequency of 12.9 GHz, the induced electric field \mathbf{E}_1 on the top layer can be decomposed into two components, \mathbf{E}_{1x} and \mathbf{E}_{1y} , perpendicular to each other. It can be remarked that \mathbf{E}_{1x} is parallel to the magnetic vector (\mathbf{H}_x) of the incident EM wave and that the cross-coupling of \mathbf{E}_{1x} and \mathbf{H}_x forms a cross-polarization conversion. Similarly, the cross-coupling between \mathbf{E}_{2x} and \mathbf{H}_x also leads to a cross-polarization switching at 15.9 GHz.

4. CONCLUSIONS

A small-size GHz-MPA, which acts as two functions of an absorber and a polarization converter, has been proven numerically and experimentally. Absorption function with almost perfect absorption at 13.9 GHz is achieved when the orientation of the unit-cell structure is symmetrical along the external electric field. Then, the symmetry of the structure is broken by rotating the resonator on the top layer, a polarization conversion function is produced with cross-reflections above 75 % in a broadband ranging from 13 to 17 GHz. The mechanism of the cross-polarization conversion is explained by the orthogonal fields induced on the asymmetric structure. The proposed MPA could be useful for novel miniaturized devices based on MMs involving wave modulation such as polarizers, filters and absorbers.

Acknowledgements. This research was funded by Vietnam National Foundation for Science and Technology Development (NAFOSTED) grant number 103.99-2018.332 and by Institute of Materials Science, Vietnam Academy of Science and Technology grant number HTCBT.01/21-21.

CRedit authorship contribution statement. Duong Thi Ha: Experiments and paper writing. Tran Quoc Ve: Simulations. Dinh Ngoc Dung: Parametric analysis. Nguyen Thi Hien: Formal analysis. Vu Thi Hong

Hanh: Formal analysis. Bui Son Tung: Conceptualization. Bui Xuan Khuyen: Methodology. Vu Dinh Lam: Supervision.

Declaration of competing interest. The authors declare that they have no known competing financial interests or personal relationships that could have appeared to influence the work reported in this paper.

REFERENCES

1. Shelby R. A., Smith D. R., and Schultz S. - Experimental verification of a negative index of refraction, *Science* **292** (2001) 77.
2. Nguyen H. T., Bui T. S., Yan S., Vandenbosch G. A., Lievens P., Vu L. D., and Janssens E. - Broadband negative refractive index obtained by plasmonic hybridization in metamaterials, *Appl. Phys. Lett.* **109** (2016) 221902.
3. Duan Z., Tang X., Wang Z., Zhang Y., Chen X., Chen M., and Gong Y. - Observation of the reversed Cherenkov radiation, *Nat. Commun.* **8** (2017) 14901.
4. Lee S. H., Park C. M., Seo Y. M., and Kim C. K. - Reversed Doppler effect in double negative metamaterials, *Phys. Rev. B* **81** (2010) 241102.
5. Veselago V. G. - The electrodynamics of substances with simultaneously negative values of ϵ and μ , *Sov. Phys. Usp.* **10** (1968) 509.
6. Smith D. R., Padilla W. J., Vier D. C., Nemat-Nasser S. C., and Schultz S. - Composite medium with simultaneously negative permeability and permittivity, *Phys. Rev. Lett.* **84** (2000) 4184.
7. Landy N. I., Sajuyigbe S., Mock J. J., Smith D. R., and Padilla W. J. - Perfect metamaterial absorber, *Phys. Rev. Lett.* **100** (2008) 207402.
8. Pendry J. B., Schurig D. and Smith D. R. - Controlling EM Fields, *Science* **312** (2006) 5781.
9. Pendry J. B. - Negative refraction makes a perfect lens, *Phys. Rev. Lett.* **85** (2000) 3966.
10. Fang N., Lee H., Sun C., and Zhang X. - Sub-diffraction-limited optical imaging with a silver superlens, *Science* **308** (2005) 534.
11. Baqir M., Choudhury P. K., Fatima T., and Ibrahim A. B. - Graphene-over-graphite-based metamaterial structure as optical filter in the visible regime, *Optik* **180** (2019) 832.
12. Bui T. S., Dao T. D., Dang L. H., Vu L. D., Ohi A., Nabatame T., Lee Y. P., Nagao T., and Hoang C. V. - Metamaterial-enhanced vibrational absorption spectroscopy for the detection of protein molecules, *Sci. Rep.* **6** (2016) 32123.
13. Bui T. S., Bui K. X., Yoo Y. J., Rhee J. Y., Kim K. W., Vu. L. D., and Lee Y. P. - Reversibly-propagation metamaterial absorber for sensing application, *Mod. Phys. Lett. B* **32** (2018) 1850044.
14. Liu N., Mesch M., Weiss T., Hentschel M., and Giessen H. - Infrared perfect absorber and its application as plasmonic sensor, *Nano Lett.* **10** (2010) 2342.
15. Khan B., Kamal B., Ullah S., Khan I., Shah J. A., and Chen J. - Design and experimental analysis of dual-band polarization converting metasurface for microwave applications, *Sci. Rep.* **10** (2020) 15393.
16. Lin B. Q., Da X. Y., Wu J. L., Li W., Fang Y. W., and Zhu Z. H. - Ultra-wideband and high-efficiency cross polarization converter based on anisotropic metasurface, *Microw. Opt. Technol. Lett.* **58** (2016) 2402.

17. Xu J., Li R., Wang S., and Han T. - Ultra-broadband linear polarization converter based on anisotropic metasurface, *Opt. express* **26** (2018) 26235.
18. Zhang F., Yang G. M., and Jin Y. Q. - Microwave Polarization Converter with Multilayer Metasurface, 2020 14th European Conference on Antennas and Propagation (EuCAP) (2020) 1.
19. Zou M., Su M., and Yu H. - Ultra-broadband and wide-angle terahertz polarization converter based on symmetrical anchor-shaped metamaterial, *Optical Materials* **107** (2020) 110062.
20. Lv F., Xiao Z., Lu X., Chen M., and Zhou Y. - Polarization Conversion and Absorption of Multifunctional All-dielectric Metamaterial Based on Vanadium Dioxide, *Plasmonics* (2020) 1.
21. Yao Y., Liao Z., Liu Z., Liu X., Zhou J., Liu G., Yi Z., and Wang J., - Recent progresses on metamaterials for optical absorption and sensing: a review, *J. Phys. D: Appl. Phys.* **54** (2021) 113002.
22. Yao Y., Zhou J., Liu Z., Liu X., Fu G., and Liu G. - Refractory materials and plasmonics based perfect absorbers, *Nanotechnology* **32** (2021) 132002.
23. Rahman S. U., Cao Q., Akram M. R., Amin F., and Wang Y., - Multifunctional polarization converting metasurface and its application to reduce the radar cross-section of an isolated MIMO antenna, *J. Phys. D: Appl. Phys.* **53** (2020) 305001.
24. Xiao S., Wang T., Liu T., Zhou C., Jiang X., and Zhang J. - Active metamaterials and metadevices: a review, *J. Phys. D: Appl. Phys.* **53** (2020) 503002.
25. Pshenay-Severin E. - Design, realization, and characterization of optical negative index metamaterials, *Diss.* (2011).
26. Aydin K., Ferry V. E., Briggs R. M., and Atwater H. A. - Broadband Polarization-Independent Resonant Light Absorption Using Ultrathin Plasmonic Super Absorbers, *Nat. Commun.* **2** (2011) 517.
27. Hajizadegan M., Ahmadi V., and Sakhdari M. - Design and Analysis of Ultrafast and Tunable All Optical Metamaterial Switch Enhanced by Metal Nanocomposite, *J. Light. Technol.* **31** (2013) 1877.
28. Tuong P. V., Park J. W., Rhee J. Y., Kim K. W., Jang W. H., Cheong H., and Lee Y. P. - Polarization-insensitive and polarization-controlled dualband absorption in metamaterials, *Appl. Phys. Lett.* **102** (2013) 081122.
29. Jia Y., Liu Y., Guo Y. J., Li K., and Gong S. - Broadband polarization rotation reflective surfaces and their applications to RCS reduction, *IEEE Trans. Antennas Propag.* **64** (1) 179-188 (2016).
30. Tuong P. V., Park J. W., Kim Y. J., Yoo Y. J., and Lee Y. P. - Broadband reflection of polarization conversion by 90° in metamaterial, *J. Korean Phys. Soc.* **64** (2014) 1116
31. Song K., Liu Y., Luo C., and Zhao X. - High-efficiency broadband and multiband cross-polarization conversion using chiral metamaterial, *J. Phys. D: Appl. Phys.* **47** (2014) 505104.
32. Ye Y., and He S. - 90° polarization rotator using a bilayered chiral metamaterial with giant optical activity, *Appl. Phys. Lett.* **96** (2010) 203501.